Title

Evaluation of penalty design in penalized maximum-likelihood image reconstruction for lesion detection

Journal

Journal of Medical Imaging, 1(3)

ISSN

2329-4302

Authors

Yang, Li

Ferrero, Andrea

Hagge, Rosalie J

et al.

Publication Date

2014-12-08

DOI

10.1117/1.jmi.1.3.035501

Peer reviewed

Journal of Medical Imaging

MedicalImaging.SPIEDigitalLibrary.org

Evaluation of penalty design in penalized maximum-likelihood image reconstruction for lesion detection

Li Yang
Andrea Ferrero
Rosalie J. Hagge
Ramsey D. Badawi
Jinyi Qi

SPIE.

Evaluation of penalty design in penalized maximum-likelihood image reconstruction for lesion detection

Li Yang,[a] Andrea Ferrero,[a] Rosalie J. Hagge,[b] Ramsey D. Badawi,[a,b] and Jinyi Qi[a,*]
[a]University of California-Davis, Department of Biomedical Engineering, One Shields Avenue, Davis, California 95616, United States
[b]UC Davis Medical Center, Department of Radiology, 4860 Y Street, Sacramento, California 95817, United States

Abstract. Detecting cancerous lesions is a major clinical application in emission tomography. Previously, we developed a method to design a shift-variant quadratic penalty function in penalized maximum-likelihood (PML) image reconstruction to improve the lesion detectability. We used a multiview channelized Hotelling observer (mvCHO) to assess the lesion detectability in three-dimensional images and validated the penalty design using computer simulations. In this study, we evaluate the benefit of the proposed penalty function for lesion detection using real patient data and artificial lesions. A high-count real patient dataset with no identifiable tumor inside the field of view is used as the background data. A Na-22 point source is scanned in air at variable locations and the point source data are superimposed onto the patient data as artificial lesions after being attenuated by the patient body. Independent Poisson noise is introduced to the high-count sinograms to generate 200 pairs of lesion-present and lesion-absent datasets, each mimicking a 5-min scan. Lesion detectability is assessed using a mvCHO and a human observer two-alternative forced choice (2AFC) experiment. The results show improvements in lesion detection by the proposed method compared with the conventional first-order quadratic penalty function and a total variation (TV) edge-preserving penalty function. [DOI: 10.1117/1.JMI.1.3.035501]

Keywords: lesion detection; penalized maximum-likelihood reconstruction; multiview channelized Hotelling observer; PET.

Paper 14089PRR received Jul. 8, 2014; accepted for publication Oct. 31, 2014; published online Dec. 8, 2014.

1 Introduction

Statistical reconstruction methods based on the penalized maximum-likelihood (PML) principle have been developed to improve image quality.[1–4] A number of metrics have been used to evaluate the quality of reconstructed PET images, such as spatial resolution, noise variance, contrast-to-noise ratio (CNR), and so on. Work has been done to design quadratic penalty functions to achieve uniform resolution[5–8] and to maximize the CNR.[9] Here, we focus on the task of lesion detection.

In previous work,[10] we proposed a method to design a shift-variant quadratic penalty function to improve lesion detectability and validated it using computer simulations. In this paper, we evaluate the benefit of the proposed penalty function for lesion detection using real data. For the benefit of clarity, we include some of the basic material that has already been previously published. A standard methodology to evaluate lesion detectability is the receiver operating characteristic curve that compares the true-positive rate versus false-positive rate for human observers.[11,12] Since human observer studies can be time consuming, numerical observers based on the signal-detection theory have been developed to reduce the cost.[13] Another benefit of using a numerical observer is that we can analytically compute the observer performance, which is critical for this work. One popular numerical observer for lesion detection in a two-dimensional (2-D) image is the channelized Hotelling observer (CHO).[14,15] With a proper choice of channels, CHO has been shown to have good correlation with human performance. To evaluate the lesion detectability in three-dimensional 3-D images, we used a multiview channelized Hotelling observer (mvCHO) to measure detection performance in the 3-D images. The mvCHO applies the conventional 2-D channels to each of the three orthogonal views (transverse, coronal, and sagittal), and then uses a Hotelling observer to combine the channel outputs into a test statistic. The mvCHO mimics the condition where a human observer examines three orthogonal views to detect a lesion.

We obtained high-count patient data using a GE DST whole-body PET scanner at UC Davis Medical Center. The patient image has no detectable lesion as verified by a radiologist (RJH). To create artificial lesions, a Na-22 point source was scanned in air at different locations and the data were superimposed onto the patient sinogram after compensating for the photon attenuation of the patient body. Corrections for random and scattered events are included in the reconstruction. We compared the lesion detection performance between PML reconstruction with the proposed penalty function, PML reconstruction with the conventional first-order quadratic penalty function, and PML reconstruction with an edge-preserving total variation (TV) penalty for a signal-known-exactly and a background-known-exactly (SKE/BKE) task.

This paper is organized as follows. In Sec. 2, we review the theory of PML image reconstruction and the method to design a shift-variant quadratic penalty function for lesion detection. In Sec. 3, we describe the method for the evaluation study. The results of the model observer study and human observer

*Address all correspondence to: Jinyi Qi, E-mail: qi@ucdavis.edu

study are presented in Sec. 4. Finally, we draw conclusions in Sec. 5.

2 Theory

2.1 *Penalized Maximum-Likelihood Image Reconstruction*

In emission tomography, the measured sinogram data $\boldsymbol{y} \in \mathcal{R}^{M\times 1}$ can be modeled as a collection of independent Poisson random variables with the expectation $\bar{\boldsymbol{y}} \in \mathcal{R}^{M\times 1}$ related to the unknown tracer distribution $\boldsymbol{x} \in \mathcal{R}^{N\times 1}$ through an affine transformation

$$\bar{\boldsymbol{y}} \equiv E[\boldsymbol{y}|\boldsymbol{x}] = \boldsymbol{P}\boldsymbol{x} + \boldsymbol{r}, \tag{1}$$

where $E[\cdot \mid \cdot]$ denotes conditional expectation, $\boldsymbol{P} \in \mathcal{R}^{M\times N}$ is the detection probability matrix with the (i,j)th element equal to the probability of detecting an event from the j'th voxel at the i'th projection element, and $\boldsymbol{r} \in \mathcal{R}^{M\times 1}$ is the expectation of the background events (scattered and random events) in the data.

PML methods estimate the unknown image $\boldsymbol{x}$ by maximizing a penalized-likelihood function,

$$\hat{\boldsymbol{x}}(\boldsymbol{y}) = \arg\max_{x\geq 0}[L(\boldsymbol{y}|\boldsymbol{x}) - \beta U(\boldsymbol{x})], \tag{2}$$

where the log-likelihood function $L(\boldsymbol{y}|\boldsymbol{x})$ is given by

$$L(\boldsymbol{y}|\boldsymbol{x}) = \sum_{i=1}^{M}(y_i \log[\boldsymbol{P}\boldsymbol{x}+\boldsymbol{r}]_i - [\boldsymbol{P}\boldsymbol{x}+\boldsymbol{r}]_i - \log y_i!). \tag{3}$$

$U(\boldsymbol{x})$ is a roughness penalty function and β is a parameter that controls the degree of regularization.

We studied two kinds of penalty functions. The first kind is the pairwise quadratic penalty

$$U(\boldsymbol{x}) = \frac{1}{2}\sum_{j=1}^{N}\sum_{l\in\mathcal{N}_j}\gamma_{jl}(x_j - x_l)^2 = \frac{1}{2}\boldsymbol{x}'R\boldsymbol{x}, \tag{4}$$

where R is a positive semi-definite matrix and ‘’ denotes the vector (or matrix) transpose. For the conventional first-order quadratic penalty, the neighborhood $\mathcal{N}_j$ contains the six nearest neighboring voxels in 3-D with all the weighting factor γ_{jl} being one, whereas the proposed penalty design method uses a larger neighborhood and seeks an optimal set of γ_{jl}'s to improve lesion detectability.

The second kind of penalty is an edge-preserving penalty based on TV[16] that is computed as

$$U(\boldsymbol{x}) = \sum_{j=1}^{N}\psi_\delta\left(\sqrt{\sum_{l\in\mathcal{N}_j}(x_j - x_l)^2}\right), \tag{5}$$

where $\psi_\delta(\cdot)$ is the hyperbola function $\psi_\delta(x) = \sqrt{x^2+\delta^2}$. When $|x| \gg \delta$, the hyperbola function approximates the absolute value function and can preserve edges. We used the first-order neighborhood (six nearest voxels in 3-D) and set $\delta = 0.01$ (around 5% of the mean image intensity).

2.2 *Penalty Design for Lesion Detection*

Here, we briefly review the major steps of the penalty design proposed in our previous work.[10] The mvCHO that we used applies 2-D frequency selective channels to each of the three orthogonal (transverse, coronal, and sagittal) views of a 3-D image and combines the channel output into a test statistic using a Hotelling observer. The test statistic of the mvCHO can be computed as

$$\eta_{\text{mvCHO}}(\hat{\boldsymbol{x}}) = \boldsymbol{z}'\boldsymbol{U}'\boldsymbol{K}^{-1}(\boldsymbol{U}\hat{\boldsymbol{x}} + \boldsymbol{n}), \tag{6}$$

where $\boldsymbol{z}$ is the expected profile of the reconstructed lesion, i.e., $\boldsymbol{z} = E[\hat{\boldsymbol{x}}|H_1] - E[\hat{\boldsymbol{x}}|H_0]$ (H_0 is the null hypothesis representing lesion absent and H_1 is the alternative hypothesis representing lesion present), $\boldsymbol{U}$ denotes a set of 2-D frequency-selective channels in three orthogonal views that mimic the human visual system, $\boldsymbol{n}$ is the internal channel noise that models the uncertainty in human detection process with mean zero and covariance $\boldsymbol{K}_N$.[14] $\boldsymbol{K}$ is the covariance of the channel outputs and can be computed as

$$\boldsymbol{K} = \frac{1}{2}\boldsymbol{U}(\Sigma_{\hat{x}|H_1} + \Sigma_{\hat{x}|H_0})\boldsymbol{U}' + \boldsymbol{K}_N, \tag{7}$$

where $\Sigma_{\hat{x}|H_1}$ and $\Sigma_{\hat{x}|H_0}$ are the covariance matrices of the PML reconstruction $\hat{x}$ under the hypotheses of H_1 and H_0, respectively. Here, we assumed the covariance to be the same for H_1 and H_0, since the presence of a small lesion has little effect on the variance of PET data.

The detection performance can be measured by the SNR of $\eta(\hat{x})$, which is given by

$$\begin{aligned}\text{SNR}^2[\eta(\hat{\boldsymbol{x}})] &= \frac{(E[\eta(\hat{\boldsymbol{x}})|H_1] - E[\eta(\hat{\boldsymbol{x}})|H_0])^2}{(\text{var}[\eta(\hat{\boldsymbol{x}})|H_1] + \text{var}[\eta(\hat{\boldsymbol{x}})|H_0])/2} \\ &= \boldsymbol{z}'\boldsymbol{U}'\boldsymbol{K}^{-1}\boldsymbol{U}z.\end{aligned} \tag{8}$$

Using theoretical approximations that have been previously derived,[17] the signal-to-noise ratio (SNR) of the mvCHO can be rapidly calculated using the fast Fourier transform

$$\text{SNR}^2_{\text{mvCHO}} \approx \left[\sum_i \frac{\tilde{U}_{k,i}\lambda_i\xi_i}{\lambda_i + \beta\mu_i}\right]\boldsymbol{K}^{-1}\left[\sum_i \frac{\tilde{U}_{k,i}\lambda_i\xi_i}{\lambda_i + \beta\mu_i}\right], \tag{9}$$

$$\boldsymbol{K} \approx \tilde{U}\,\text{diag}\left[\frac{\lambda_i}{(\lambda_i + \beta\mu_i)^2}\right]\tilde{\boldsymbol{U}}' + \boldsymbol{K}_N, \tag{10}$$

where $\tilde{U}$ are the Fourier coefficients of the channels, $\{\xi_i\}_{i=1}^N$ is the Fourier transform of the expected lesion profile, $\{\lambda_i\}_{i=1}^N$ and $\{\mu_i\}_{i=1}^N$ are the Fourier coefficients of the column vector of the Fisher information matrix $\boldsymbol{F} = \boldsymbol{P}'\text{diag}[1/\bar{\boldsymbol{y}}]\boldsymbol{P}$ and penalty matrix R corresponding to the voxel at the center of the lesion. In the above equations, $[\alpha_j]$ denotes a column vector with the j'th element being α_j and $\text{diag}[\alpha_j]$ denotes a diagonal matrix with the (j,j)'th element being α_j. The j'th column vector of the Fisher information matrix can be computed by first forward projecting the j'th unit vector $\boldsymbol{e}_j$ using the system matrix P to obtain $\boldsymbol{P}\boldsymbol{e}_j$, then following with a weighted back projection to get $\boldsymbol{P}'\text{diag}[1/\bar{\boldsymbol{y}}](\boldsymbol{P}\boldsymbol{e}_j)$. Rearranging the j'th column vector as a 3-D image and taking its 3-D Fourier transform result in $\{\lambda_i\}_{i=1}^N$.

By decomposing the quadratic penalty function into pairwise penalties as given in Eq. (4), the column vector of the penalty matrix R corresponding to the voxel j at the center of the lesion can be viewed as a weighted sum of basic penalty kernels

$$\boldsymbol{Re}_j = \sum_{l \in \mathcal{N}_j} \gamma_{jl} \boldsymbol{b}_{jl}, \tag{11}$$

where $\boldsymbol{b}_{jl}$ is a vector and can be viewed as an image which only has nonzero values at pixels j, l, and the symmetric pixel of l with respect to pixel j. For example, the first-order penalty only contains the horizontal and vertical kernels

$$\boldsymbol{b}_{\text{horizontal}} = \begin{bmatrix} 0 & 0 & 0 \\ -1 & 2 & -1 \\ 0 & 0 & 0 \end{bmatrix}, \quad \boldsymbol{b}_{\text{vertical}} = \begin{bmatrix} 0 & -1 & 0 \\ 0 & 2 & 0 \\ 0 & -1 & 0 \end{bmatrix}. \tag{12}$$

Taking the Fourier transform of the pairwise penalty kernel $\boldsymbol{b}_{jl}$, we can express μ_i as a function of γ_{jl}:

$$\mu_i^j = \sum_l \gamma_{jl} \mu_i^l, \tag{13}$$

where μ_i^l is the frequency response of the l'th pairwise penalty with basis kernel b_{jl}. Note that μ_i in Eq. (9) becomes μ_i^j and can vary from voxel to voxel, and $\text{SNR}^2_{\text{mvCHO}}$ in Eq. (9) becomes a function of γ_{jl}. For a given dataset, we can estimate the weighting factors γ_{jl} to maximize the lesion detectability at voxel j

$$\{\hat{\gamma}_{jl}\} = \arg \max_{\gamma_{jl} \geq 0} \text{SNR}^2_{\text{mvCHO}} \tag{14}$$

and repeat this procedure for all voxels. The final penalty function is computed as

$$\boldsymbol{x}'\boldsymbol{R}\boldsymbol{x} = \sum_{j=1}^{N} \sum_{l \in \mathcal{N}_j} \frac{\hat{\gamma}_{jl} + \hat{\gamma}_{lj}}{2} (x_j - x_l)^2 \tag{15}$$

to ensure that $\boldsymbol{R}$ is symmetric.

Equation (14) can be evaluated using a MATLAB® function "fmincon" and a detailed pseudocode outlining the penalty design procedure can be found in the previous work.[10] It is worth noting that while the estimated $\hat{\gamma}_{jl}$ depends on the value of β, the product $\beta\hat{\gamma}_{jl}$ and the maximum value of $\text{SNR}_{\text{mvCHO}}$ are independent of the value of β. Therefore, without loss of generality, we always set β to one in the penalty design.

3 Method

To generate lesion present and lesion absent images with known ground truth, we obtained high-count, lesion-free patient data as the normal background. The high-count data were obtained from a 60-min dynamic PET scan of a 64-year-old female patient with a 5-mCi FDG injection. The scan was performed on a GE DST whole-body scanner in the fully 3-D mode and covered the heart, breasts, and part of the lungs and liver. We summed the last 45-min PET data to create a high-count sinogram with 800 million events. The reconstructed patient image was verified by a radiologist (RJH) to be free of lesion and can be used as the normal background. To create lesion-present sinogram data, we scanned a ^{22}Na point source at 27 positions on a $3 \times 3 \times 3$ grid using a reference block shown in Fig. 1. The sinograms of the point source data were first attenuated by the patient attenuation factors obtained from the patient's CT scan, and then added to the patient sinogram as artificial lesions. After excluding 7-point source locations that were either outside the patient body or at implausible positions, we had 20 artificial lesions in total. Figure 2 shows one sample reconstruction with an artificial lesion inside the liver. To simulate a typical 5-min scan, independent Poisson noise was introduced to the high-count sinograms to generate noisy data sets each with 90 million expected total number of events. Two hundred pairs of noisy data sets with and without lesion were generated for the observer studies.

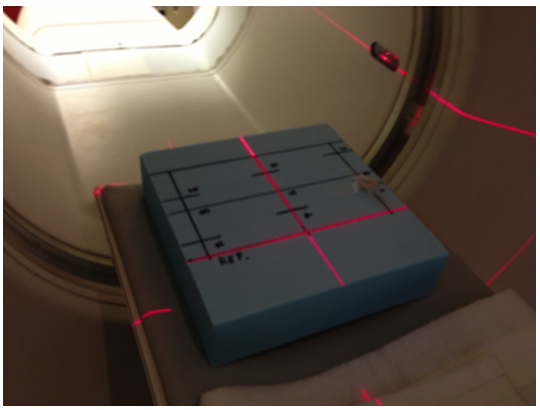

Fig. 1 Point source placed on a coarse grid on top of a reference block.

The noisy data were independently reconstructed by the PML reconstruction with the first-order quadratic penalty function, the proposed penalty function, and the TV edge-preserving penalty function. All three reconstruction algorithms used the same distance-driven projector.[18] Patient attenuation factors were incorporated in the forward model in all reconstructions. Random and scattered sinograms were estimated using the manufacturer provided software and were included in the reconstruction. All images were reconstructed using a $192 \times 192 \times 47$ image array with $3.65 \times 3.65 \times 3.27$ mm^3 voxels. We implemented a MAP-EM algorithm with 300 iterations to reconstruct the image using the quadratic penalties.[19] For the TV penalty, a preconditioned conjugate gradient algorithm with 100 iterations was used for faster convergence. One iteration in either algorithm takes about 1 min.

To measure the lesion detection performance, we used the mvCHO with three difference-of-Gaussian channels.[20] The internal noise was modeled as independent Gaussian noise with zero mean and covariance $\boldsymbol{K}_N = 10^{-4.5}\boldsymbol{I}$, where $\boldsymbol{I}$ is the identity matrix.[21] We used the theoretical expression of the mvCHO SNR in Eq. (9) to find the optimal β value for the first-order quadratic penalty function. To find the optimal penalty that provides the highest SNR for the lesion detection, we first computed the optimum weighting factor $\hat{\gamma}_{jl}$ based on Eq. (14) for the 20 lesion locations and then assigned the value of γ_{jl} to other voxels using the nearest neighbor interpolation. For the case when the lesion location is unknown, one will need to compute the optimum weighting factors on a finer grid.[22] We chose a large neighborhood $\mathcal{N}_j$ that included the 92 nearest voxels. Because of symmetry, only 46 independent γ_{jl} need to be determined at each location. The computation took about 10 min for each location using one 2.0GHz Intel CPU. With the estimated $\hat{\gamma}_{jl}$, we can form the column vector of the penalty matrix $\boldsymbol{R}$ corresponding to the voxel at the center

Fig. 2 Three orthogonal slices of the sample reconstruction with a superimposed lesion in the liver as shown in the center of the yellow circle: (a) transverse slice, (b) sagittal slice, (c) coronal slice.

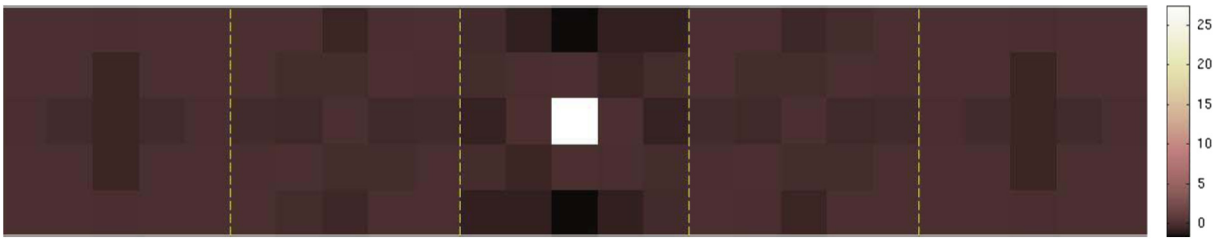

Fig. 3 The estimate $\hat{\gamma}_{jl}$ image for the lesion location shown in Fig. 2. The three-dimensional (3-D) penalty kernel only has nonzero values in a $5 \times 5 \times 5$ region. All five transverse slices of the penalty kernel are shown and voxel j is the center white voxel.

of lesion. Figure 3 showed the estimated $\hat{\gamma}_{jl}$ image for the lesion location shown in Fig. 2. We also computed the Monte Carlo SNR using the mean and the covariance of the channel outputs obtained from the 200 pair reconstructed images using different penalty functions.[23] The Monte Carlo results were compared with the theoretical predictions.

A human observer (LY) performed a two-alternative forces choice (2AFC) experiment to verify the numerical observer results. At each time, a pair of reconstructed images, with and without a tumor, was presented to the human observer and the observer was asked to select the image with a tumor. For every lesion location and reconstruction algorithm combination, the observer read 200 pair reconstructed images. The 200 image pairs were divided into two groups each with 100 samples. We use the first 10 image pairs in each group for training, and the remaining 90 image pairs for testing. The resulting percent correct in the 2AFC test was converted into the SNR by[24]

$$\text{SNR} = 2\text{erf}^{-1}(2\text{PC} - 1). \tag{16}$$

We performed McNemar's test on the human observer 2AFC results to evaluate the statistical significance of the difference between the proposed penalty function and the first-order quadratic penalty function and the TV edge-preserving penalty fucntion.[25] Each 2AFC experiment was considered as a Bernoulli experiment with two possible outcomes (0 for incorrect choice and 1 for correct choice). The outcomes of a pair of 2AFC experiments between any two methods can be sorted into four categories as shown in Table 1. From the observed value of N_1 to N_4, we computed the p-value of McNemar's test.

Table 1 Four categories of the two-alternative forced choice (2AFC) experiment outcomes.

Penalty A	Penalty B	Number of cases
Correct	Correct	N_1
Wrong	Wrong	N_2
Correct	Wrong	N_3
Wrong	Correct	N_4

4 Results

We picked three representative lesion locations [Figs. 4(a) to 4(c)] and plotted the SNR values for different reconstruction algorithms as a function of β. We compared the Monte Carlo SNR of the mvCHO with the theoretical predications for the first-order quadratic penalty and proposed penalty functions in Figs. 4(d) to 4(f). Note that the SNR of the proposed penalty function is independent of the β value; hence, we only show the Monte Carlo result at $\beta = 1$. In general, the Monte Carlo results match the theoretical predictions very well and both show improvements of the proposed penalty function over the first-order penalty. Furthermore, we observed that the optimal β value of the first-order quadratic penalty function to achieve the maximum SNR varied for different lesion locations, which meant multiple reconstructions with different β values would be necessary when using the first-order quadratic penalty

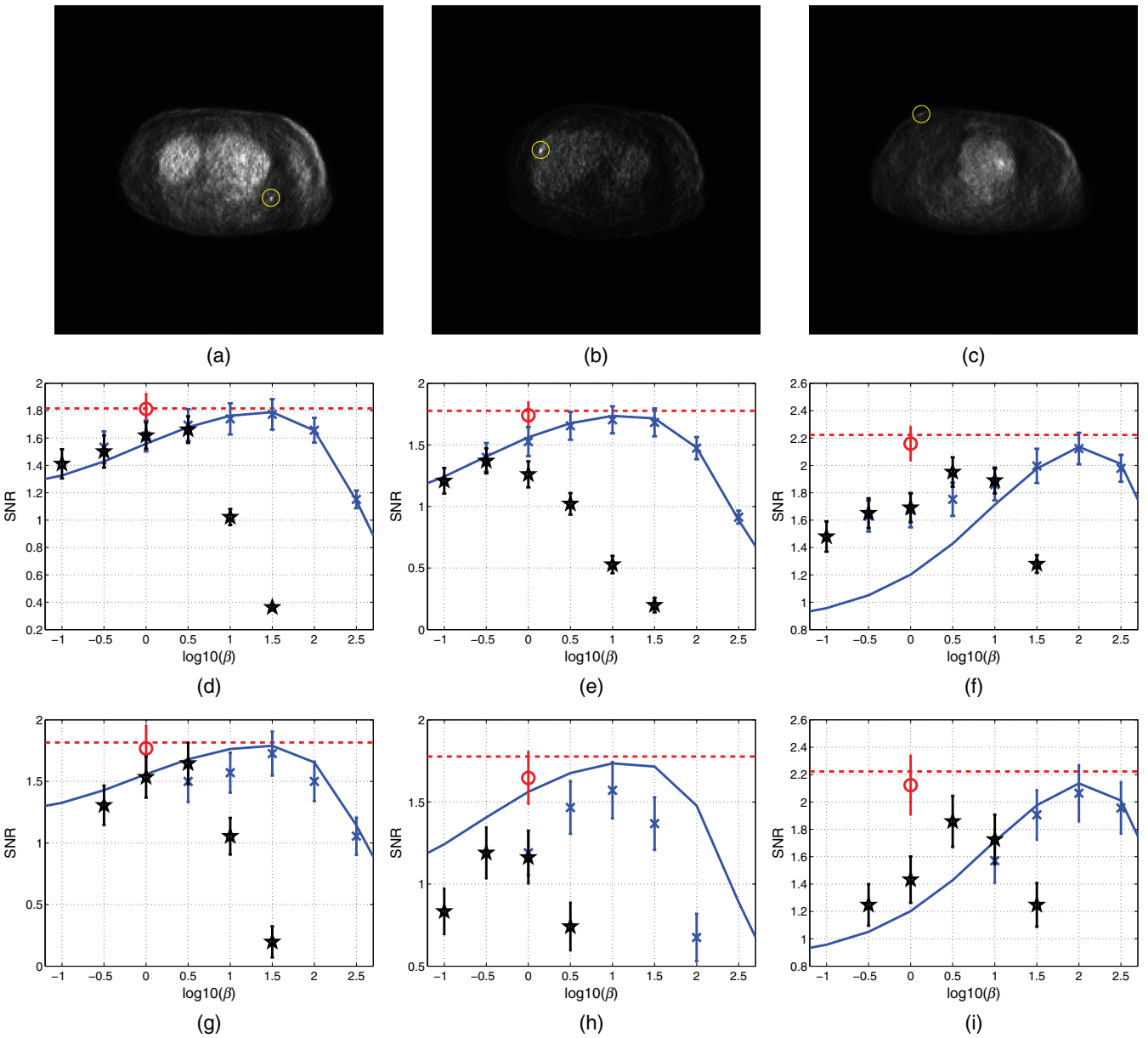

Fig. 4 Comparison of the lesion detectability at three representative locations. Top row (a–c): reconstructed images showing a lesion at the center of each yellow circle. Middle row (d–f): plot of mvCHO SNR's as a function of β. The theoretical prediction for the first-order quadratic penalty is shown by the solid blue lines and the theoretical prediction for the proposed penalty is shown by the dashed red lines. The Monte Carlo results of the first-order quadratic penalty are marked by "×"s and those of the proposed penalty by "o"s. The Monte Carlo results of the TV edge-preserving penalty are marked by black "⋆"s. The error bars indicate plus and minus one standard deviation. Bottom row (g–i): plot of human observer SNR as a function of β with comparison to theoretical predictions (lines). The human observer results of the first-order quadratic penalty are marked by "×"s; those of the proposed penalty by "o"s; and those of the TV penalty by "⋆"s.

function to achieve the optimal lesion detection. With the proposed optimized penalty function, we can obtain the highest detection performance at all locations using one set of regularization parameters. We also plotted the Monte Carlo SNR of PML reconstruction using the edge-preserving TV penalty in Figs. 4(d) to 4(f). Comparing the peak SNR achieved by the TV penalty with that by the proposed penalty, we did not find any improvement for lesion detectability by using the edge-preserving penalty over the quadratic penalties, which is consistent with previous studies.[26,27] We note that while we plotted the SNR of different penalty functions on a common β axis, it is only fair to compare the peak SNR achieved by each penalty function because the β value has a different scale for each penalty function.

The SNR of the human observer as a function of β at three sample locations is shown in Figs. 4(g) to 4(i). The human performances follow the same trends as those of the theoretical prediction and Monte Carlo reconstructions.

In Fig. 5, we compared the human observer results of the proposed penalty with that of the first-order quadratic penalty

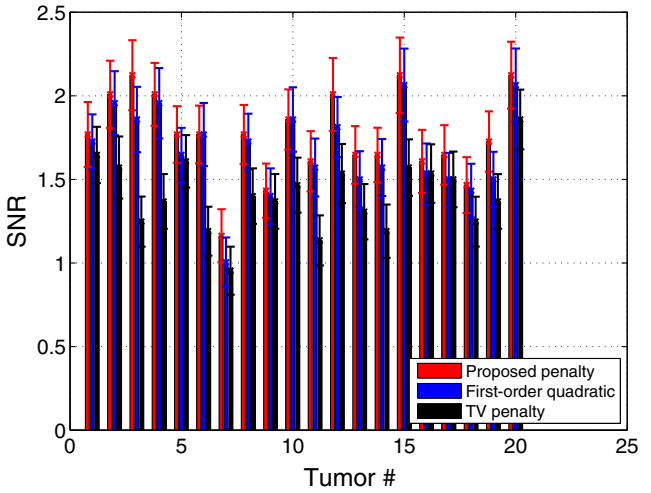

Fig. 5 Comparison of the human observer results for the three penalty functions each under their respective optimal β value determined by the multiview channelized Hotelling observer (mvCHO) at the 20 lesion locations.

Table 2 The McNemar's test results.

	Proposed penalty versus first-order quadratic penalty	Proposed penalty versus TV penalty
N_1	3025	2863
N_2	260	245
N_3	180	342
N_4	135	150
p-value	0.0066	<0.00001

and the edge-preserving TV penalty each under their respective optimal β value predicted by the mvCHO for the 20 locations. The resulting values of $N_1 - N_4$ for the McNemar's test are shown in Table 2 with the p-values given in the last row of Table 2. The results show that the proposed penalty function achieved the highest SNR for lesion detection at almost all tumor locations.

5 Conclusion

We have evaluated the detection performance of our proposed penalty design method using real-patient data with artificially inserted lesions. Numerical observer and human observer results show that the proposed penalty outperforms the first-order quadratic penalty function and the edge-preserving TV penalty function for the specific SKE–BKE lesion detection task, system configuration, and reconstruction paradigm used in this work. In the future, we will apply the proposed method to real clinical datasets.

Acknowledgments

The authors would like to acknowledge Dr. Charles Stearns, GE Healthcare for his assistance on the GE PET toolbox. The authors also thank the anonymous reviewers for their constructive suggestions that helped to improve the quality of the manuscript. This work was supported by the National Institutes of Health under Grant No. R01 EB 000194.

References

1. J. A. Fessler, "Penalized weighted least-squares image reconstruction for positron emission tomography," *IEEE Trans. Med. Imaging* **13**, 290–300 (1994).
2. E. U. Mumcuoglu et al., "Fast gradient-based methods for Bayesian reconstruction of transmission and emission PET images," *IEEE Trans. Med. Imaging* **13**, 687–701 (1994).
3. J. A. Fessler and A. O. Hero, "Penalized maximum-likelihood image reconstruction using space-alternating generalized EM algorithms," *IEEE Trans. Image Process.* **4**, 1417–1429 (1995).
4. C. A. Bouman and K. Sauer, "A unified approach to statistical tomography using coordinate descent optimization," *IEEE Trans. Image Process.* **5**, 480–492 (1996).
5. J. W. Stayman and J. A. Fessler, "Regularization for uniform spatial resolution properties in penalized-likelihood image reconstruction," *IEEE Trans. Med. Imaging* **19**, 601–615 (2000).
6. J. Qi and R. M. Leahy, "Resolution and noise properties of MAP reconstruction for fully 3-D PET," *IEEE Trans. Med. Imaging* **19**, 493–506 (2000).
7. J. W. Stayman and J. A. Fessler, "Compensation for nonuniform resolution using penalized-likelihood reconstruction in space-variant imaging systems," *IEEE Trans. Med. Imaging* **23**, 269–284 (2004).
8. H. R. Shi and J. A. Fessler, "Quadratic regularization design for 2-D CT," *IEEE Trans. Med. Imaging* **28**, 645–656 (2009).
9. J. Qi and R. M. Leahy, "A theoretical study of the contrast recovery and variance of MAP reconstructions from PET data," *IEEE Trans. Med. Imaging* **18**, 293–305 (1999).
10. L. Yang et al., "Regularization design in penalized maximum-likelihood image reconstruction for lesion detection in 3-D PET," *Phys. Med. Biol.* **59**, 403–419 (2014).
11. D. R. Gilland et al., "An evaluation of maximum likelihood-expectation maximization reconstruction for SPECT by ROC analysis," *J. Nucl. Med.* **33**, 451–457 (1992).
12. J. Llacer et al., "Results of a clinical receiver operating characteristic study comparing filtered backprojection and maximum likelihood estimator images in FDG PET studies," *J. Nucl. Med.* **34**, 1198–1203 (1993).
13. H. H. Barrett et al., "Model observers for assessment of image quality," *Proc. Natl. Acad. Sci. U. S. A.* **90**, 9758–9765 (1993).
14. J. Yao and H. H. Barrett, "Predicting human performance by a channelized Hotelling model," *Proc. SPIE* **1768**, 161–168 (1992).
15. K. J. Myers and H. H. Barrett, "Addition of a channel mechanism to the ideal-observer model," *J. Opt. Soc. Am. A* **4**, 2447–2457 (1987).
16. L. Rudin, S. Osher, and E. Fatemi, "Nonlinear total variation based noise removal algorithms," *Phys. D: Nonl. Phen.* **60**, 259–268 (1992).
17. J. Qi, "Analysis of lesion detectability in Bayesian emission reconstruction with nonstationary object variability," *IEEE Trans. Med. Imaging* **23**, 321–329 (2004).
18. B. De Man and S. Basu, "Distance-driven projection and backprojection in three dimensions," *Phys. Med. Biol.* **49**, 2463–2475 (2004).
19. A. De Pierro, "A modified expectation maximization algorithm for penalized likelihood estimation in emission tomography," *IEEE Trans. Med. Imaging* **14**, 132–137 (1995).
20. C. K. Abbey, H. H. Barrett, and D. W. Wilson, "Observer signal-to-noise ratios for the ML-EM algorithm," *Proc. SPIE* **2712**, 47–58 (1996).
21. C. K. Abbey and H. H. Barrett, "Human- and model-observer performance in ramp-spectrum noise: effect of regularization an object variability," *J. Opt. Soc. Am. A* **18**, 473–488 (2001).
22. L. Yang, J. Zhou, and J. Qi, "Regularization design for breast lesion detection in penalized maximum-likelihood image reconstruction,"

in *Proc. IEEE Int. Symp. on Biomedical Imaging*, pp. 626–629, IEEE, Piscataway, New Jersey (2012).
23. H. H. Barrett and K. J. Myers, *Foundations of Image Science*, John Wiley and Sons, Hoboken, New Jersey (2004).
24. A. E. Burgess, "Comparison of receiver operating characteristic and forced choice observer performance measurement methods," *Med. Phys.* **22**, 643–655 (1995).
25. D. G. Altman, *Practical Statistics for Medical Research*, Chapman and Hall/CRC, Boca Raton, Florida (1990).
26. J. Qi, "Comparison of lesion detection and quantification in MAP reconstruction with Gaussian and non-Gaussian priors," *Int. J. Biomed. Imaging* **2006**, 1–10 (2006).
27. J. Nuyts et al., "Performance of MAP reconstruction for hot lesion detection in whole-body PET/CT: an evaluation with human and numerical observers," *IEEE Trans. Med. Imaging* **28**, 67–73 (2009).

Li Yang received his BS degree in precision instrumentation from Tianjin University, China, in 2009. Currently, he is pursuing his PhD degree in biomedical engineering at the University of California, Davis, under the supervision of professor Jinyi Qi. His research interests include image quality analysis and statistical image reconstruction for emission tomography.

Andrea Ferrero is a graduate student in biomedical engineering at the University of California, Davis. His research interests include quantification in PET and SPECT, hybrid modalities, and translational molecular imaging. His research is funded by an HHMI international predoctoral fellowship.

Rosalie J. Hagge is a clinical professor of radiology and nuclear medicine at UC Davis Medical Center. She has degrees in computer science/engineering, and received her MD in 1988 from Washington University in St. Louis. She did postgraduate studies in medical informatics and digital medical imaging at Washington University. She completed residency in nuclear medicine at the WU in 1993, and diagnostic radiology at Duke University in 1998, then joined Duke University as an assistant professor. In 2002, she moved to UC Davis, where her duties are primarily clinical and teaching. She serves as a clinical consultant to biomedical engineering, and participates in both clinical and molecular imaging research.

Ramsey D. Badawi is an associate professor of radiology and biomedical engineering, and chief of nuclear medicine at the University of California, Davis. He has been working in PET and medical imaging since the early 1990s. His primary research interests include PET hardware and software developments and translational imaging.

Jinyi Qi is a professor in the Department of Biomedical Engineering at the University of California, Davis. He received his PhD degree in electrical engineering from University of Southern California in 1998. Prior to joining the faculty of University of California, Davis, he was a research scientist in the Department of Functional Imaging at the Lawrence Berkeley National Laboratory. His research interests include statistical image reconstruction, medical image processing, image quality evaluation, and imaging system optimization.